Extended Kalman Filtering Based Parameter Estimation and Drift Compensation for A MEMS Rate Integrating Gyroscope

Zhongxu Hu, Barry J Gallacher

School of Mechanical and System Engineering, Newcastle University, Newcastle upon Tyne, UK

Abstract:

This paper presents an offline extended Kalman filtering based parameter identification and drift compensation for a MEMS ring vibratory gyroscope. Damping and stiffness imperfections are the major error sources in MEMS vibratory gyroscopes. In the rate integrating operation mode, where angle is output instead of angular velocity as in the case of the rate gyroscope, parameter identification is an essential prerequisite for any feedback control and compensation algorithm to minimize angle drift and other errors. The proposed EKF method provides five estimates for the resonator DC loop gain, and another four parameters related to the non-proportional damping and aniso-elasticities. The method is based on the slowly varying averaged dynamic model expressed in terms of orbital elements. The averaging methodology offers important advantages over similar attempts based directly on the dynamic model expressed in terms of fast time varying displacement and velocity of vibration. Firstly, the observed measurements are subjected to significantly lower levels of noise as a consequence of the narrowband demodulation process employed in the calculation of the orbital elements. Secondly, the EKF requires much lower update rate due to the slowly varying nature of the augmented states. These advantages result in a more accurate estimation, improved stability performance and the possibility for real time implementation of the EKF. Numerical simulation and offline implementation of the EKF using experimental gyroscope operation data are provided to validate the proposed method. Moreover, the identified damping imperfections have been used in the drift compensation control in a DSP based real time rate integrating gyroscope control system. Ultimately, the maximum angular drift has been reduced to 1 degree per second. Spectrum analysis shows the angle drift error is dominated by 4^{th} harmonics caused by dynamics not included in models of the conventional gyroscope model.

Keywords:

MEMS rate integrating gyroscope; Parameter estimation; Extended Kalman filter; Drift compensation.

1. Introduction

Gyroscopes are an essential element in inertial measurement units (IMUs) and inertial navigation systems (INS) widely used in unmanned aerial vehicles (UAV). They are also a common component in both industrial and consumer electronics where they provide localization, orientation and other navigation data. The MEMS vibratory gyroscope is attractive because of its small size and ease of integration within a digital system. However, there are still major challenges, for example, structural aniso-elasticities and non-proportional damping caused by fabrication tolerance limits and material inhomogeneity. These imperfections result in undesired coupling between the vibration modes and interfere with the desired Coriolis coupling. This undesired coupling manifests primarily as angular drift in rate integrating gyroscopes. Theoretically, the RIG has unlimited bandwidth and range, though, this benefit may be compromised by bandwidth of the electronic control loops and communication link used to transfer sensor output. While the upper cut-off rate of RIG can be promoted by using fast hardware, such as FPGA based control system, the lower threshold rate that the RIG can respond to is determined by the precession angle dependent bias error and minimum rate threshold caused by damping and stiffness imperfections. Sophisticated control algorithms developed to accommodate the imperfections have attracted lots of research interests, such as adaptive control [1, 2], and compensation via state feedback

control [3, 4, 5]. These control and compensation strategies require accurate modelling and real time parameter identification. However, parameter estimation [6-8] for MEMS vibratory gyroscope is challenging because the numerical values of the imperfections span at least six orders of magnitude. As reported in [9], the simple least-squares estimation based on frequency response data often leads to biased errors. An instrumental variable method [10] together with perturbation theory may provide correct identification of the mass, stiffness matrices, and the non-proportional damping. However, this method is based on a block of input-output data, it is slow and not suited to real-time on line adaptive control. A nonlinear observer is proposed in [11, 12] for parameter estimation for angular drift compensation in a hemispherical vibratory gyroscope. The design process requires choices of two nonlinear functions that determine the asymptotical stability of the observer. However, existence of the appropriate nonlinear functions is not guaranteed.

The extended Kalman filter (EKF) is a model based recursive estimation algorithm for nonlinear systems that provides estimate of state variables of interests. It can be readily extended to parameter identification by treating unknown parameters as extended state variables. It is ideally suited to parameter estimation for the vibratory gyroscope since the mathematical model of the gyroscope is sufficiently well known. The process is recursive and based only on the current measurements and prediction, making it convenient to form an adaptive control to compensate for imperfections in the gyroscope. The EKF uses linearization approximation for the nonlinear system dynamics and requires very high estimation update rate so that the errors caused by linearization approximation can be ignored. This is particularly challenging for MEMS vibratory gyroscopes where typical operation occurs at resonance frequencies in the KHz range.

There are a few published reports of Kalman filtering (UKF) applied to MEMS gyroscope parameter estimation [13-15]. In these cases the estimation is based on the fast time varying dynamics expressed in a Cartesian coordinate system. The challenges faced with this approach are: Firstly, in practical applications, the observed measurements are subjected to severe wideband electronic noise from the preamplifier circuits. Secondly, the resonator of the gyroscope usually operate at resonant frequencies in the KHz range. Therefore, the sampling rate and update rate of estimation becomes impractically high when considered in conjunction with the heavy calculation costs involved in implementing the EKF. For this reason, none of these attempts provided experimental test results except digital simulation.

This paper proposes an EKF based on the slowly varying averaged dynamic model that provides parameter identification for a rate integrating vibratory gyroscope. This method has advantages over the conventional EKF for vibratory gyroscope systems. The measurements available for the estimation process are obtained from a narrowband demodulation algorithm with significantly reduced noise. The system states to be estimated are slowly time varying thus eliminating the need for high estimation update rate without violating the linearization approximation condition.

In order to validate the proposed EKF parameter identification and drift compensation, the EKF is tested using a full numerical simulation of the rate integrating gyroscope control system. In addition the EKF is tested offline using operational data from an actual real time controlled MEMS rate integrating gyroscope in order to assess the robustness of the parameter estimation to practical noisy measurements and model uncertainties in real gyroscope devices. Finally, the EKF estimated damping imperfection parameters are used to determine the right amount of state feedback in the DSP based real time control system in order to reduce the non-proportional damping caused angular drift error. As a result of this compensation a maximum angular drift of less than 1 degree per second is reported. This represents the best reported performance so far for a MEMS rate integrating gyroscope. Furthermore, a spectrum analysis of angle output of an actual RIG shows the second harmonic resulting from damping imperfection has been reduced significantly by feedback compensation using the estimation results from the offline EKF, while the fourth harmonics remains unchanged. The results shown in

this paper clearly reveals the existence and influence of higher order imperfections caused by the direct drive, gain mismatch etc. that are not covered in the conventional averaged model [19].

2. Basic algorithm of EKF

EKF is a discrete Kalman filter adapting to nonlinear system estimation through linearization. The algorithm can be briefly described as follows [16]. If the nonlinear dynamics of the system of interest $\dot{\boldsymbol{X}} = f'(\boldsymbol{X}, \boldsymbol{u})$ is well modelled, it can be readily discretised using the well-known Euler method. The discrete form state and output difference equations are written as:

$$\begin{cases} \boldsymbol{X}_k = \boldsymbol{X}_{k-1} + f'(\boldsymbol{X}_{k-1}, \boldsymbol{u}_{k-1}, \boldsymbol{w}_{k-1})\Delta t \equiv f(\boldsymbol{X}_{k-1}, \boldsymbol{u}_{k-1}, \boldsymbol{w}_{k-1}) \\ \boldsymbol{z}_k = h(\boldsymbol{X}_k, \boldsymbol{u}_k, \boldsymbol{v}_k) \end{cases} \tag{1}$$

Where $\boldsymbol{X}_k$, $\boldsymbol{z}_k$ represent the state variables and available output measurements respectively, $\boldsymbol{u}_k$ is the control input vector. The terms $\boldsymbol{w}_k$ and $\boldsymbol{v}_k$ are zero mean process and measurement white noise, with covariance matrix Q_k and R_k respectively. The Kalman filter generates optimal state estimate $\widehat{\boldsymbol{X}}_k$ with a minimum variance. It can be readily extended to accommodate parameter estimation by treating the parameters as auxiliary states where $\boldsymbol{X}_k = \boldsymbol{X}_{k-1}$.

The recursive computation consists of two steps:

Step 1: prediction

$$\begin{cases} \widehat{\boldsymbol{X}}_k^- = f\left(\widehat{\boldsymbol{X}}_{k-1}, h\left(\widehat{\boldsymbol{X}}_{k-1}, \boldsymbol{u}_{k-1}\right), \boldsymbol{u}_{k-1}, 0\right) \\ P_k^- = A_k P_{k-1} A_k^T + W_k Q_{k-1} W_k^T \end{cases} \tag{2}$$

Step 2: correction

$$\begin{cases} K_k = P_k^- H_k^T (H_k P_k^- H_k^T + V_k R_k V_k^T)^{-1} \\ \widehat{\boldsymbol{X}}_k = \widehat{\boldsymbol{X}}_k^- + K_k \left(\boldsymbol{z}_k - h\left(\widehat{\boldsymbol{X}}_k^-, \boldsymbol{u}_k, 0\right)\right) \\ P_k = (I - K_k H_k) P_k^- \end{cases} \tag{3}$$

Here P_k is the covariance of the state estimation error, A_k and H_k are the process and measurement Jacobians at step k respectively. Matrix A is the Jacobian matrix of the state difference equation $f(\boldsymbol{X}_{k-1}, \boldsymbol{u}_{k-1}, \boldsymbol{w}_{k-1})$, defined as:

$$A_{[i,j]} = \frac{\partial f_{[i]}}{\partial \boldsymbol{X}_{[j]}}(\boldsymbol{X}_{k-1}, \boldsymbol{u}_{k-1}, 0) \tag{4}$$

H is the Jacobian matrix of the output function $h(\boldsymbol{X}_k, \boldsymbol{u}_k, \boldsymbol{v}_k)$ with respect to $\boldsymbol{X}$:

$$H_{[i,j]} = \frac{\partial h_{[i]}}{\partial \boldsymbol{X}_{[j]}}(\boldsymbol{X}_k, \boldsymbol{u}_k, 0) \tag{5}$$

Similarly, W is Jacobian matrix of $f(\boldsymbol{X}_{k-1}, \boldsymbol{u}_{k-1}, \boldsymbol{w}_{k-1})$ with respect to $\boldsymbol{w}$, and V is Jacobian matrix of partial derivatives of $h(\boldsymbol{X}_k, \boldsymbol{u}_k, \boldsymbol{v}_k)$ with respect to $\boldsymbol{v}$. For simplicity, in the implementation of the EKF, W, V are seen as identity matrices. In order to apply the Kalman filter for parameter estimation the system dynamics must be established and some output measurement data must be available.

3. Dynamics of the MEMS vibratory ring gyroscope

Vibratory gyroscopes exploit Coriolis coupling between a pair of spatially orthogonal vibration modes. In the ideal case the two vibration modes have mode shapes related through rotation, identical natural frequencies and identical damping parameters. In practical devices structural imperfections always exist. As described in [17] if the structural imperfections can be treated as perturbations then the dynamics of the ring gyroscope, when

centrifugal and angular acceleration terms are neglected, can be described in terms of the idealised in-plane flexural modes of the ring of circumferential order *n* by

$$\begin{bmatrix}\ddot{p}\\ \ddot{q}\end{bmatrix}+2\xi_0\omega_0\begin{bmatrix}1+\gamma_1 & \gamma_2\\ \gamma_2 & 1-\gamma_1\end{bmatrix}\begin{bmatrix}\dot{p}\\ \dot{q}\end{bmatrix}+\omega_0^2\begin{bmatrix}1+\mu_1 & \mu_2\\ \mu_2 & 1-\mu_1\end{bmatrix}\begin{bmatrix}p\\ q\end{bmatrix}=\begin{bmatrix}F_p/m\\ F_q/m\end{bmatrix}+\begin{bmatrix}2\Omega_z\dot{q}\\ -2\Omega_z\dot{p}\end{bmatrix} \tag{6}$$

Here p, q are the modal displacements of the pair of *n*th circumferential modes described in a rectangular coordinate system X, Y, Z with the Z axis corresponding to the polar axis of the ring. The X and Y axes correspond to the modal coordinates p and q, respectively. The orientation of the X and Y axes are defined such that the X axis is aligned with respect to an arbitrary drive electrode. Most often the *n*=2 modes are chosen for gyroscopic applications. For the perfect case the natural frequency, modal mass and modal damping ratio are denoted by ω_0, m and ξ_0. Imperfections in damping and stiffness are denoted by γ_1, γ_2 and μ_1, μ_2, respectively. Coriolis coupling between the modal coordinates p and q occurs when an angular velocity Ω_z is applied about the polar axis of the ring. External electrostatic forces are denoted F_p, F_q . Note that higher order contributions resulting from mass imperfections are not considered.

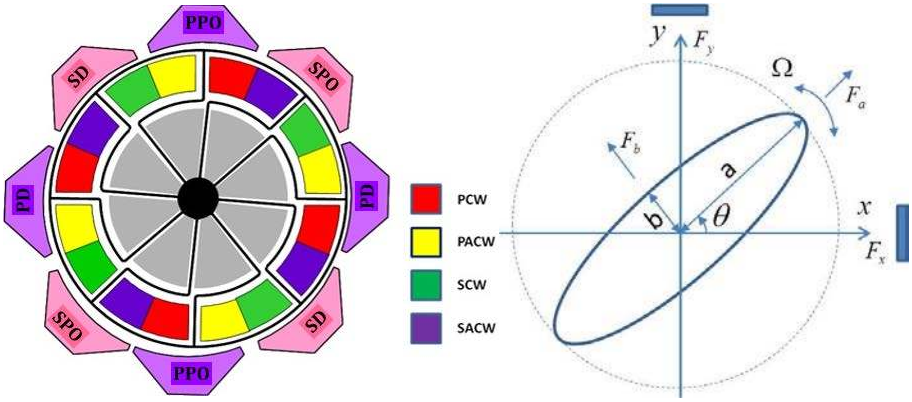

Figure 1, (a), Schematic of micro-ring vibrating gyroscope. (b), Vibration in elliptic coordinate system.

The state variables p, q and excitation forces F_p, F_q in equation (6) are only accessed and manipulated via an electronic interface circuit. In order to implement any control, the practical dynamic model needs to take into account the gains of the interface circuit. The gyroscope in this study has a planar ring structure and uses capacitive actuation and sensing. The electrostatic force is calculated using the energy stored in the capacitor

$$W=\frac{1}{2}CV^2=\frac{1}{2}C_0\frac{d}{d+x'}V^2 \tag{7}$$

Here d is the nominal gap of the capacitor, x' is the displacement from equilibrium, $C=\varepsilon\frac{A}{d+x'}$ and $C_0=\varepsilon\frac{A}{d}$ are dynamic and nominal capacitances. The electrostatic force is

$$\mathrm{F}=-\frac{\partial W}{\partial x'}\approx-\frac{1}{2}\frac{C_0}{d}V^2+\frac{C_0V^2}{d^2}x' \tag{8}$$

The voltage $V=V_{dc}+V_{ac}$ in equation (8) consists of a DC bias V_{dc} and an alternating drive signal V_{ac}. The second term has negative electrostatic spring softening effect, while the first displacement independent term is used as an excitation force. Since the alternating excitation voltage V_{ac} is kept much smaller than DC bias V_{dc}, the alternative excitation force can be approximated as $f_e\approx\eta_dV_{ac}$, where $\eta_d=V_{dc}\frac{C_0}{d}$ is the electromechanical conduction gain.

The capacitive vibration sensing is described as motional current that is proportional to the velocity of vibration:

$$i = \frac{\partial CV}{\partial t} = V\frac{\partial C}{\partial t} + C\frac{\partial V}{\partial t} \approx V_{dc}\frac{\partial C}{\partial t} = V_{dc}\frac{\partial C}{\partial x'}\frac{\partial x'}{\partial t} = \eta_s\frac{\partial x'}{\partial t} \tag{9}$$

An electrical signal can be extracted from this motional current by using an electronic preamplifier circuit. A trans-impedance amplifier converts the motional current into vibration velocity, whilst a charge amplifier converts it into displacement. As this study uses a charge amplifier, the feedback capacitance together with η_s determine the detection gain. The displacement signal is described as $x = \frac{\eta_s}{C_F}x'$.

The equation of motion in terms of sensed signals x, y corresponding to the transduced displacements and the alternating drive voltage signals f_x, f_y is described as

$$\begin{bmatrix}\ddot{x}\\ \ddot{y}\end{bmatrix} + 2\xi_0\omega_0\begin{bmatrix}1+\gamma_1 & \gamma_2\\ \gamma_2 & 1-\gamma_1\end{bmatrix}\begin{bmatrix}\dot{x}\\ \dot{y}\end{bmatrix} + \omega_0^2\begin{bmatrix}1+\mu_1 & \mu_2\\ \mu_2 & 1-\mu_1\end{bmatrix}\begin{bmatrix}x\\ y\end{bmatrix} = k_{ds}\begin{bmatrix}f_x\\ f_y\end{bmatrix} + \begin{bmatrix}2\Omega_z\dot{x}\\ -2\Omega_z\dot{y}\end{bmatrix} \tag{10}$$

The gain $k_{ds} = \frac{\eta_d\eta_s}{mC_F}$ is a combination of both the drive and sense electronic interface circuits. In addition to the four damping and stiffness imperfection parameters, the estimation algorithm must also include the gain k_{ds}.

Kalman filter based parameter estimation applied to gyroscopes are reported in the literature [13-15]. However, the methods reported are applied directly to the dynamic equation defined in equation (6). A major disadvantage of such approach is that the state variables are directly measured displacement and velocity signals which are subjected to severe noise contamination. Furthermore, estimation requires a very high sampling rate due to the fast time varying displacement and velocity state variables. In this paper, it is proposed to base the estimation on the amplitude and phase model. The amplitude and phase state variables are obtained by a signal demodulation process within a very narrow bandwidth thus improving the noise reduction. Furthermore, the state variables are now slowly time varying resulting in reduced sampling rate and estimation update rate. Consequently it is possible to implement the estimation in real time practically.

4. Averaged slow varying model

In general, the control of the vibratory rate integrating gyroscope consists of control modules for resonance tracking, energy sustain and quad nulling. The design and analysis of control is more conveniently performed by expressing the equation of motion in terms of amplitude and phase, instead of rectangular coordinates as in equations (6) and (10). Transformation of the equation of motion from rectangular coordinates to time averaged elliptic polar coordinates has been described in detail by [18-19].

The transformation process starts by defining state variables as displacement and velocity of vibration for the model defined by equation (10)

$$u = \begin{bmatrix}x\\ y\\ \dot{x}\\ \dot{y}\end{bmatrix} \tag{11}$$

For simplicity, the Coriolis coupling is not included in this brief description. Equation (10) can be written in state space vector form

$$\dot{u} = \begin{bmatrix}0 & \mathrm{I}\\ -\omega_0^2\mathrm{I} & 0\end{bmatrix}u + \begin{bmatrix}f_1\\ f_2\end{bmatrix} \tag{12}$$

where

$$f_1 = 0,$$
$$f_2 = -2\xi_0\omega_0\begin{bmatrix}1+\gamma_1 & \gamma_2\\ \gamma_2 & 1-\gamma_1\end{bmatrix}\begin{bmatrix}\dot{x}\\ \dot{y}\end{bmatrix} - \begin{bmatrix}0 & -2\Omega\\ 2\Omega & 0\end{bmatrix}\begin{bmatrix}\dot{x}\\ \dot{y}\end{bmatrix} - {\omega_0}^2\begin{bmatrix}\mu_1 & \mu_2\\ \mu_2 & -\mu_1\end{bmatrix}\begin{bmatrix}x\\ y\end{bmatrix} + \begin{bmatrix}f_x\\ f_y\end{bmatrix} \tag{13}$$

The coordinate transformation expresses the system equation in terms of slow time varying orbital elements described in figure 1b, which are defined as:

$$z = \begin{bmatrix} a \\ b \\ \theta \\ \varphi \end{bmatrix} \tag{14}$$

Here φ denotes the phase shift between the resultant drive F_a and response component $a(t)$ in the major axis. The transformation from state vector u in the rectangular coordinate system to state vector z in the elliptic polar coordinate system is denoted as $u = g(t, z)$, refereeing to figure 1, which is described as

$$\begin{aligned} x(t) &= a\cos\theta\cos(\omega t + \varphi) - b\sin\theta\sin(\omega t + \varphi) \\ y(t) &= a\sin\theta\cos(\omega t + \varphi) + b\cos\theta\sin(\omega t + \varphi) \\ \dot{x}(t) &= \omega(-a\cos\theta\sin(\omega t + \varphi) - b\sin\theta\cos(\omega t + \varphi)) \\ \dot{y}(t) &= \omega(-a\sin\theta\sin(\omega t + \varphi) + b\cos\theta\cos(\omega t + \varphi)) \end{aligned} \tag{15}$$

Equation (10) can be rewritten in terms of the slowly time varying orbital elements using the transformation defined by equation (15).

$$\dot{a} = -a\xi_0\omega_0(1 + \gamma_1\cos 2\theta + \gamma_2\sin 2\theta) - \frac{1}{2}b\omega_0(\mu_1\sin 2\theta - \mu_2\cos 2\theta) + f_a \tag{16}$$

$$\dot{b} = -b\xi_0\omega_0(1 - \gamma_1\cos 2\theta - \gamma_2\sin 2\theta) + \frac{1}{2}a\omega_0(\mu_1\sin 2\theta - \mu_2\cos 2\theta) + f_b \tag{17}$$

$$\dot{\theta} = -\Omega_z + \frac{a^2+b^2}{a^2-b^2}\xi_0\omega_0(\gamma_1\sin 2\theta - \gamma_2\cos 2\theta) - \frac{ab}{a^2-b^2}\omega_0(\mu_1\cos 2\theta + \mu_2\sin 2\theta) + f_\theta \tag{18}$$

$$\dot{\varphi} = \frac{1}{2}\omega_0\frac{a^2+b^2}{a^2-b^2}(\mu_1\cos 2\theta + \mu_2\sin 2\theta) + \frac{ab}{a^2-b^2}2\xi_0\omega_0(-\gamma_1\sin 2\theta + \gamma_2\cos 2\theta) + \omega_0 - \omega + f_\phi \tag{19}$$

Where $f_a, f_b, f_\theta, f_\phi$ are effective forces on the elliptic elements caused by f_x, f_y, they have the form of proportional velocity and skew symmetric displacement feedback [20, 21] for energy sustain and quad nulling respectively.

$$\begin{bmatrix} f_x \\ f_y \end{bmatrix} = \beta\begin{bmatrix} 1 & 0 \\ 0 & 1 \end{bmatrix}\begin{bmatrix} \dot{x} \\ \dot{y} \end{bmatrix} + \alpha\begin{bmatrix} 0 & 1 \\ -1 & 0 \end{bmatrix}\begin{bmatrix} x \\ y \end{bmatrix} \tag{20}$$

The effective forces in the elliptic frame are described as:

$$f_a = -k_{ds}\left(\frac{1}{2}a\beta - \frac{1}{2\omega}b\alpha\right)\sin\varphi \tag{21}$$

$$f_b = -k_{ds}\left(\frac{1}{2}b\beta - \frac{1}{2\omega}a\alpha\right)\sin\varphi \tag{22}$$

$$f_\theta = -k_{ds}\frac{\alpha}{2\omega}\cos\varphi \tag{23}$$

$$f_\phi = -k_{ds}\left(\frac{\beta}{2} + \frac{ab}{2\omega(a^2-b^2)}\alpha\right)\cos\varphi \tag{24}$$

Equations (21) - (24) show the equivalent forces on the averaged model are affected by the locked orbital phase φ. A digital PLL is implemented based on a DSP that is able to lock the orbital phase to -90 degrees with an error less than 0.05 degrees. When the resonance tracking control has kept the orbital phase $\varphi = -\frac{\pi}{2}$, f_θ and f_ϕ become zero. It means the control of form (20) do not interfere neither with the precession angle nor the resonance frequency. Both forces f_a, f_b reach maximum at resonance.

In order to implement the feedback controls in the elliptic coordinate system, it is necessary to accurately measure the four state variables. The capacitive sensing circuit measures the displacement of the two vibration modes $x(t), y(t)$. Each of the vibration signals is decomposed into a pair of in-phase and quadrature components via a digital signal orthogonal demodulation process:

$$\begin{cases} x(t) = C_x \cos(\omega t) + S_x \sin(\omega t) \\ y(t) = C_y \cos(\omega t) + S_y \sin(\omega t) \end{cases} \tag{25}$$

The demodulation results C_x, S_x, C_y, S_y are slow time varying comparing with the displacements, and they have significantly less noise because of the low pass filtering used in the narrow band demodulation process. Combining equations (15) and (25), there are five invariables [19] can be calculated using the demodulation results C_x, S_x, C_y, S_y:

$$\begin{cases} Q = 2\big(C_x S_y - C_y S_x\big) = 2ab \\ S = 2\big(C_x C_y + S_x S_y\big) = (a^2 - b^2)\sin 2\theta \\ R = {C_x}^2 + {S_x}^2 - {C_y}^2 - {S_y}^2 = (a^2 - b^2)\cos 2\theta \\ L_R = {C_x}^2 - {S_x}^2 + {C_y}^2 - {S_y}^2 = (a^2 - b^2)\cos 2\varphi \\ L_I = 2\big(C_x S_x + C_y S_y\big) = (a^2 - b^2)\sin 2\varphi \end{cases} \tag{26}$$

The "slow" time-varying variables of the vibration, the amplitudes a, b, phase φ and precession angle θ, are readily calculated from the five invariables. Thereafter, they are used in the control of the sensor system and as sensor output. Lynch's method described in [19][5] uses the total energy and angular momentum. In this paper, the amplitudes a, b, phase φ are directly chosen as the controlled variables for the amplitude, quad, and frequency locking loops respectively. Note that the forces in equations (21) -(24) are equivalent (time averaged) forces projected on the elliptic frame from the state feedback control (20), which is implemented in the x-y frame by the driving electrodes.

The actual implementation of state feedback control (20) relies on the reconstruction of system states $[x, y, \dot{x}, \dot{y}]$. Given the measurement results a, b, θ, φ and the internal phase reference $\sin(\omega t)\ \cos(\omega t)$, , the system states are readily reconstructed using equation (15). When the PLL is locked,

$$\begin{cases} x(t) = a\cos\theta \sin(\omega t) + b\sin\theta \cos(\omega t) \\ y(t) = a\sin\theta \sin(\omega t) - b\cos\theta \cos(\omega t) \\ \dot{x}(t) = \omega(a\cos\theta \cos(\omega t) - b\sin\theta \sin(\omega t)) \\ \dot{y}(t) = \omega(a\sin\theta \cos(\omega t) + b\cos\theta \sin(\omega t)) \end{cases} \tag{27}$$

The feedback control (20) is therefore readily formed as combination of the internal phase reference, measurements of the orbiting elements and control gains β and α:

$$\begin{cases} f_x = \big(-\hat{\beta} b + \alpha a\big)\sin\theta \sin(\omega t) + \big(\hat{\beta} a - \alpha b\big)\cos\theta \cos(\omega t) \\ f_y = -\big(-\hat{\beta} b + \alpha a\big)\cos\theta \sin(\omega t) + \big(\hat{\beta} a - \alpha b\big)\sin\theta \cos(\omega t) \end{cases} \tag{28}$$

Here $\hat{\beta} = \beta\omega$, gains β, α are respectively the outputs of two conventional PID control loops used to stabilize the amplitude of the major axis a to a specified value, and to suppress the minor axis b. The same procedure applies for the formulations of angular steering and feedback compensation, as detailed in [4].

The digital control system based on the averaged model (16)-(19), and principle of measurements (25)-(26) is described in the block diagram of figure 2. It consists of three control loops for resonance control, vibration sustaining and quad nulling. It also features a module for precession angle steering for the purposes of tuning and calibration. This RIG control system is implemented on a high performance DSP platform.

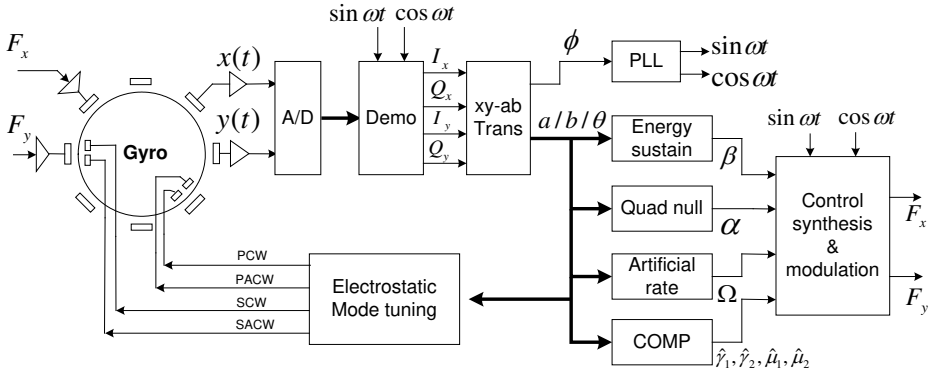

Figure 2, Block diagram of the gyroscope control system.

As shown in equation (18), when amplitude of the minor axis b is minimized by quad nulling, the influence of stiffness imperfections μ_1, μ_2 on angular precession is negligible for small frequency split gyros [17]. Angle drift is mainly caused by damping imperfections γ_1, γ_2 [5][22]. Setting the right amount of compensation is the key to reduce the damping imperfection caused angle drift. In this paper, EKF is only a way to find the unknown parameters, so that we can set the correct gain for the velocity feedback to compensate for the damping imperfections. The EKF does not replace the PID control loops for the control of the major axis, minor axis and resonance tracking.

5. EKF implementation

The objective of the EKF is to estimate the augmented states $[a(t), b(t), \gamma_1, \gamma_2, \mu_1, \mu_2, k_s]'$ corresponding to the major and minor axes of the ellipse, stiffness and damping imperfections, and the gain of the resonator. The EKF uses two measurements, $[a, b]'$, in the estimation process. Note here the precession angle θ is seen as a known parameter to the EKF, although it is varying due to precession caused by external rate input. The two control inputs are the feedback gains for vibration sustaining and quad nulling, β and α. By applying the Euler method with a sampling rate Δt, the discrete model for the estimation system is described as:

$$\begin{cases} a_k = \mathrm{f}'_a(a_{k-1}, b_{k-1}, \gamma_{1,k}, \gamma_{2,k}, \mu_{1,k}, \mu_{2,k}, k_{s,k}, \Delta t) + w_1 \\ b_k = \mathrm{f}'_b(a_{k-1}, b_{k-1}, \gamma_{1,k}, \gamma_{2,k}, \mu_{1,k}, \mu_{2,k}, k_{s,k}, \Delta t) + w_2 \\ \gamma_{1,k} = \gamma_{1,k-1} + w_3 \\ \gamma_{2,k} = \gamma_{2,k-1} + w_4 \\ \mu_{1,k} = \mu_{1,k-1} + w_5 \\ \mu_{2,k} = \mu_{2,k-1} + w_6 \\ k_{s,k} = k_{s,k-1} + w_7 \end{cases} \tag{29}$$

Here

$$\mathrm{f}'_a(a_{k-1}, b_{k-1}, \gamma_{1,k}, \gamma_{2,k}, \mu_{1,k}, \mu_{2,k}, k_{s,k}, \Delta t) = a_{k-1} + \Big\{-a_{k-1}\xi_0\omega_0\big(1 + \gamma_{1,k-1}\cos 2\theta + \gamma_{2,k-1}\sin 2\theta\big) - \frac{1}{2}b_{k-1}\omega_0\big(\mu_{1,k-1}\sin 2\theta - \mu_{2,k-1}\cos 2\theta\big) + k_{ds,k-1}\Big(\frac{1}{2}a_{k-1}\beta - \frac{1}{2\omega}b_{k-1}\alpha\Big)\Big\}\Delta t + w_1$$

$$\mathrm{f}'_b(a_{k-1}, b_{k-1}, \gamma_{1,k}, \gamma_{2,k}, \mu_{1,k}, \mu_{2,k}, k_{s,k}, \Delta t) = b_{k-1} + \Big\{-b_{k-1}\xi_0\omega_0\big(1 - \gamma_{1,k-1}\cos 2\theta - \gamma_{2,k-1}\sin 2\theta\big) + \frac{1}{2}a_{k-1}\omega_0\big(\mu_{1,k-1}\sin 2\theta - \mu_{2,k-1}\cos 2\theta\big) + k_{ds,k-1}\Big(\frac{1}{2}b_{k-1}\beta - \frac{1}{2\omega}a_{k-1}\alpha\Big)\Big\}\Delta t + w_2$$

The Jacobian matrix A is given by:

$$A = \begin{bmatrix} A_{11} & A_{12} & -a_{k-1}\xi_0\omega_0\Delta t\cos 2\theta & -a_{k-1}\xi_0\omega_0\Delta t\sin 2\theta & -\frac{1}{2}b_{k-1}\omega_0\Delta t\sin 2\theta & \frac{1}{2}b_{k-1}\omega_0\Delta t\cos 2\theta & \Delta t\left(\frac{1}{2}a_{k-1}\beta - \frac{1}{2\omega}b_{k-1}\alpha\right) \\ A_{21} & A_{22} & b_{k-1}\xi_0\omega_0\Delta t\cos 2\theta & b_{k-1}\xi_0\omega_0\Delta t\sin 2\theta & \frac{1}{2}a_{k-1}\omega_0\Delta t\sin 2\theta & -\frac{1}{2}a_{k-1}\omega_0\Delta t\cos 2\theta & \Delta t\left(\frac{1}{2}b_{k-1}\beta - \frac{1}{2\omega}a_{k-1}\alpha\right) \\ 0 & 0 & 1 & 0 & 0 & 0 & 0 \\ 0 & 0 & 0 & 1 & 0 & 0 & 0 \\ 0 & 0 & 0 & 0 & 1 & 0 & 0 \\ 0 & 0 & 0 & 0 & 0 & 1 & 0 \\ 0 & 0 & 0 & 0 & 0 & 0 & 1 \end{bmatrix}$$

where,

$$A_{11} = 1 + \left\{-\xi_0\omega_0\left(1 + \gamma_{1,k-1}\cos 2\theta + \gamma_{2,k-1}\sin 2\theta\right) + \tfrac{1}{2}k_{ds,k-1}\beta\right\}\Delta t \tag{30}$$

$$A_{12} = \left\{-\tfrac{1}{2}\omega_0\left(\mu_{1,k-1}\sin 2\theta - \mu_{2,k-1}\cos 2\theta\right) - \tfrac{1}{2\omega}k_{ds,k-1}\alpha\right\}\Delta t \tag{31}$$

$$A_{21} = \left\{\tfrac{1}{2}\omega_0\left(\mu_{1,k-1}\sin 2\theta - \mu_{2,k-1}\cos 2\theta\right) - \tfrac{1}{2\omega}k_{ds,k-1}\alpha\right\}\Delta t \tag{32}$$

$$A_{22} = 1 + \left\{-\xi_0\omega_0\left(1 - \gamma_{1,k-1}\cos 2\theta - \gamma_{2,k-1}\sin 2\theta\right) + \tfrac{1}{2}k_{ds,k-1}\beta\right\}\Delta t \tag{33}$$

Two of the orbiting elements, a, b are chosen as measurement outputs to implement the EKF. The measurement Jacobian matrix is:

$$H = \begin{bmatrix} 1 & 0 & 0 & 0 & 0 & 0 & 0 \\ 0 & 1 & 0 & 0 & 0 & 0 & 0 \end{bmatrix}$$

$w_1 \sim w_7$ in equation (29) are the noise covariance for each state, together with the noise covariance $v_1 \sim v_2$ for the two available measurements will be used as tuning parameters of the EKF.

6. Simulation results

The proposed EKF based parameter identification is validated through a full numerical simulation of the RIG system. It incorporates the dynamics of the gyroscope, phase-locked loop for resonance tracking, velocity feedback for energy sustaining, displacement feedback for quad nulling. The EKF parameter identification is fed with closed-loop control gains and state values of the controlled RIG. The Simulink block diagram is shown in figure 3. The control and detection subsystems are described in the control system block diagram in figure 2. The EKF subsystem is implemented in Matlab script as a recursive loop, described in section 5. The dynamic parameters were set close to that of a practical MEMS gyroscope. A resonant frequency of 14 kHz, quality factor of 22000, non-proportional damping γ_1, γ_2 of 0.02 and 0.03 respectively, and stiffness imperfections $\mu_1,\ \mu_2$ of -30e-6 and -40e-6 respectively have been used in the simulation. The frequency split between the two modes is 0.5 Hz. The resonator DC gain is set to 1.1e5.

Tuning of the EKF parameters e.g, the dynamic model (process) noise covariance matrix Q_k, and zero mean measurement noise covariance matrix R_k need to be tuned to ensure fast convergence of the estimates and with sufficient accuracy. This is a critical task in ensuring a successful implementation for this application where the values of the estimates range from e-5 to e5. Orthogonal demodulation using a digital FIR filter to obtain the measurements is advantageous as it removes most of the ripple and noise. As a result, the observations are subjected to low noise influences and the measurement noise covariance matrix R_k can be set to a relatively low value of $[0.0001, \quad 0.0001]$. The process noise covariance matrix Q_k corresponding to $w_1 \sim w_7$ in equation (29) is set to $[0.0001 \quad 0.0001 \quad 0.0001 \quad 1 \quad 1 \quad 0.01 \quad 0.01 \quad e7]$ which reflects the range of uncertainties of the five parameters to be estimated. During the estimation process, a high rate input causing fast angular precession speeds up the transient process of the EKF. The convergence results for the selected EKF parameter settings are shown in figure 4 and figure 5.

In the numerical simulation, no un-modelled dynamics of the gyroscope can affect the EKF. The sampling rate is high so the linearization error is small. The EKF gives a very accurate estimation of the gyroscope parameters.

As shown in figure 4 and figure 5, the EKF estimates the damping imperfections γ_1, γ_2 to be 0.02 and 0.03 respectively, and stiffness imperfections $\mu_1,\ \mu_2$ to be -30e-6 and -40e-6 respectively. They are exactly the set values.

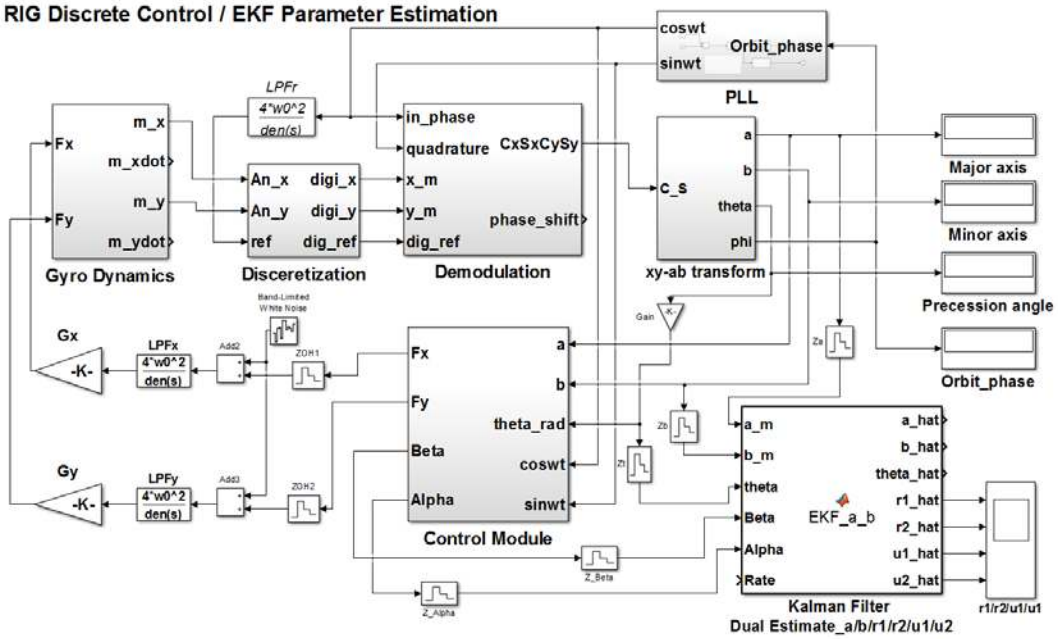

Figure 3, Block diagram of the EKF embedded in the RIG control system

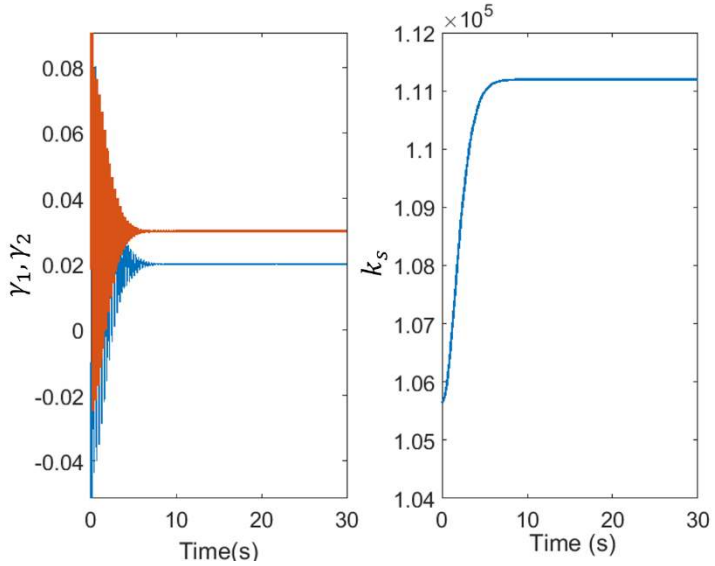

Figure 4, Estimates of damping imperfections γ_1, γ_2 and resonator gain k_s

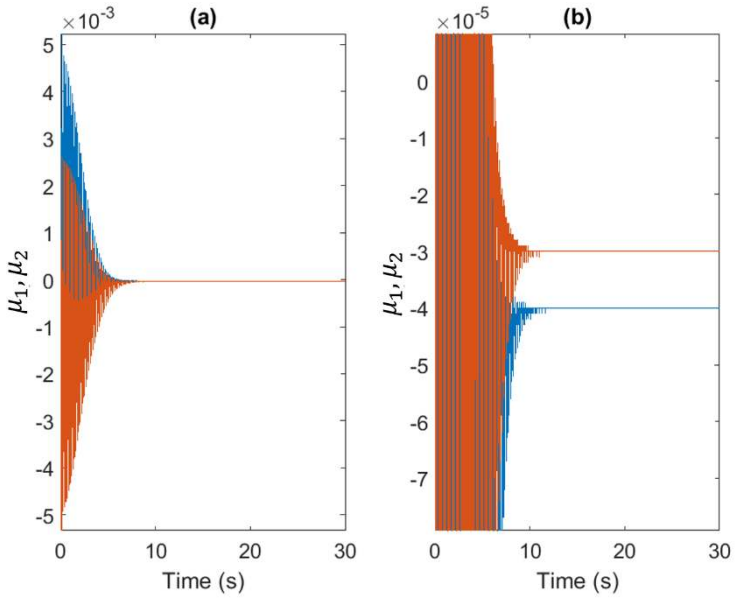

Figure 5, Estimates of stiffness imperfections μ_1, μ_2, (b) reveals the accuracy of the estimates

7. Experimental EKF and compensation tests

The numerical simulation has shown that in the ideal case the EKF is accurate enough to provide parameter estimation stretching from a few micro to half a million given accurate system model and clean measurement observation. However, in practical applications, there exists higher level of noise in the observation, and un-modelled dynamics exist. These can affect the performance of the EKF applied to practical EMS gyroscope control systems. This section provides test results of the offline implemented EKF fed by operation data from a practical gyroscope.

The proposed EKF has been experimentally tested with a practical high performance MEMS gyroscope. The electrode configuration of the planar ring type capacitive gyroscope is shown in figure 1. It uses electrostatic drive and charge amplifier sensing interface circuit, and has a DC bias of 25 V. The resonant frequencies of the two modes have a nominal value of 14.195 kHz when the frequency split has been electrostatically reduced from 1.5Hz to less than 10 mHz [21] as shown in figure 6. It is critical to minimize the frequency split so that angle precession in the presence of the remaining imperfections occurs at a relative low rate input. The frequency split between the modes serves as the threshold level for the requested minimum rate input. From the frequency response test shown in figure 6, the quality factor is measured to be 22000 and the total damping imperfection is measured to be about 0.03 of the average [21]. The resonator DC gain is determined from the frequency response by the relation

$$k_s = \frac{\omega^2}{Q} k_{in/out} \tag{34}$$

and has a value of 2000000. $k_{in/out}$ denotes the input output voltage gain at resonance.

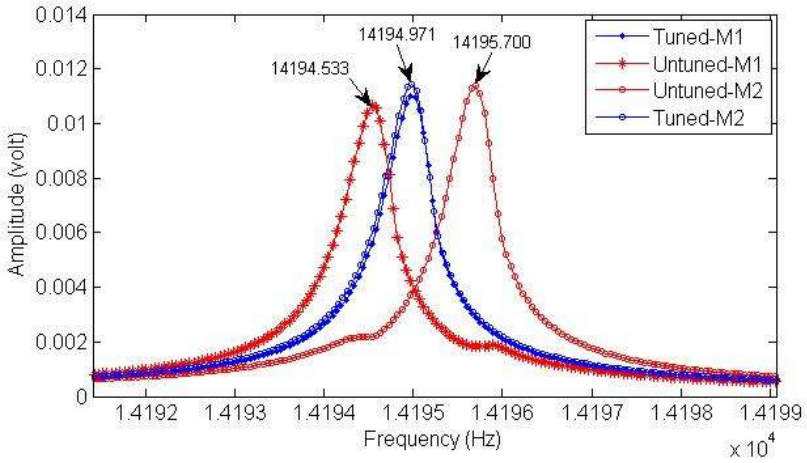

Figure 6, Frequency response before and after electrostatic mode tuning.

Operational data from a practical gyroscope to be applied to the offline EKF is collected when the RIG is under continuous angular precession. It is preferable to apply a rate as low as possible, which ensures the linearization approximation error won't become excessive and affect the stability of the EKF. On the other hand, before the correct damping parameters are predicted by the proposed offline EKF, and proper compensation gains are set in the real time control, a lower rate will result in the RIG fail to precess continuously due to large angular drift error. As shown in figure 8, the peak-to-peak angular drift of the uncompensated RIG is about 9 degrees per second. It is a precession angle dependent bias error appearing as second harmonics. Another important concept for RIG is the rate threshold, at which the measured angle will not track the true rotation angle. A simple analytical expression for rate threshold caused by anisodamping is given in theoretical work by Prikhodko, Igor P., et al [22]. Rate threshold caused by frequency mistuning is addressed in [17], though the effect is negligible when quadrature control is used in the RIG control system [5] and frequency mistuning is extremely small.

In this test, an artificial rate of 12 degrees per second is used that allows continuous angle precession. When the gyroscope is under rotation, system input output data is widespread which leads to fast convergence of the recursive process of the EKF. The offline EKF is fed with operation data of 6 full rotations for the recursive process to converge. This amount of data takes about 5 minutes to collect.

The EKF is primarily tested offline by a MATLAB program using experimentally observed measurements a, b and control data β, α collected from the DSP based control system. The sampling time is set to 0.1 s. The EKF fed with operation data of 6 full rotations takes two minutes to converge. The estimation results are shown in figure 7. The stiffness imperfections are shown to be very close to zero which reflects the fine-tuned gyro frequency split of less than 10mHz. However, estimation for the stiffness imperfections is not yet able to resolve mistuning in the sub-micro range. DC loop gain of the resonators is 2.19e6, and the damping imperfections γ_1 and γ_2 are estimated to be 0.035 and -0.006, respectively.

Though the EKF is implemented offline, it can be used as a powerful tool in the calibration stage to identify important parameters of actual gyroscopes. The offline EKF gives accurate estimation of damping imperfections, which allows the feedback control in the form (35) to set the right amount of compensation to suppress angular drift. Estimated stiffness values μ_1, μ_2 can be used for frequency tuning by electrostatic tuning. As for this device, the mode mistuning is already very small (10 mHz), the EKF wasn't able to identify such small values, as shown in figure 7.

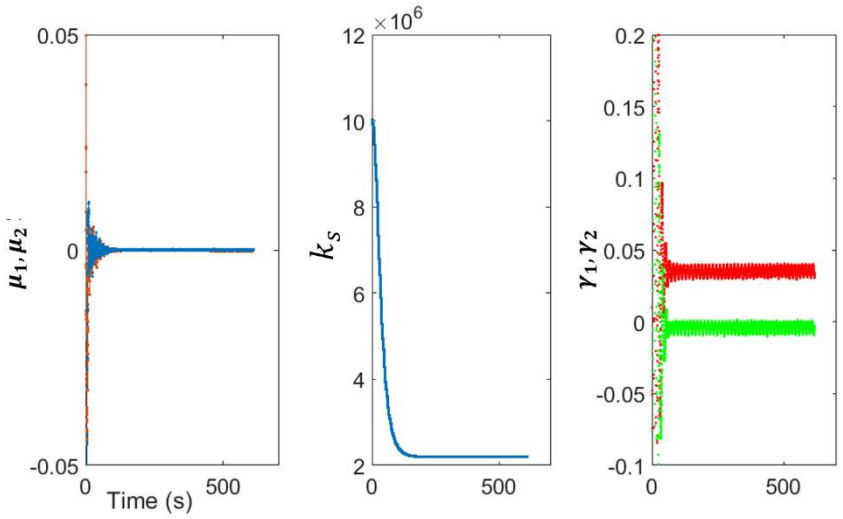

Figure 7, EKF estimation on experimental gyro data.

Angle drift is the major error in rate integrating gyroscope, which is mainly caused by the damping imperfections. With the estimation results, the damping imperfections induced angle drift can be readily compensated by a velocity feedback control added to the existing controls described in (20).

$$\begin{bmatrix} f_{c\_x} \\ f_{c\_y} \end{bmatrix} = \beta \begin{bmatrix} -\gamma_1 & -\gamma_2 \\ -\gamma_2 & \gamma_1 \end{bmatrix} \begin{bmatrix} \dot{x} \\ \dot{y} \end{bmatrix} \tag{35}$$

The results from the EKF based parameter identification have been successfully used in the feedback control to minimize angle drift error. When the quad nulling control is in place to minimize the amplitude of the minor axis, and the mode mistuning is electrostatically tuned to a small value, it is clear from equation (18) that the angle drift caused by the stiffness imperfections are very small relative to the damping imperfections. The effect of the stiffness imperfections on the angle drift is negligible. The estimated damping imperfections γ_1, γ_2 and DC gain k_s are used to calculate the optimal amount of state feedback to minimize the rate fluctuation. When the gyroscope is under constant rate input, the fluctuation magnitude of sensed rate indicates the maximum angle drift. Figures 8 to 10 show the experimental results after minimising the damping imperfections and demonstrate the effectiveness of the EKF as a powerful tool in the process of reducing angular drift error caused by damping imperfections. In figures 8 to 10 the rate input was maintained constant. Four different levels of damping compensation are shown. Case 1 is before any feedback compensation is applied and it shows the highest angular rate fluctuation of 9 °/s. The required energy sustain control has the highest swing along the precession cycle, and the EKF estimate shows γ_1, γ_2 to be 0.035 and -0.006, respectively. Simulated angle drift using estimated parameters in case #1 is shown to fit the test data closely. Case 2 shows an over-compensated damping γ_1 of -0.016. The angular drift is reduced to 8 °/s. In case 3, γ_1, γ_2 are shown to be reduced to near zero and 0.006, respectively. The maximum angle drift is now about 1.5 °/s. Finally, in case 4 both damping terms are compensated very close to zero. The angle drift is reduced to less than 1 °/s.

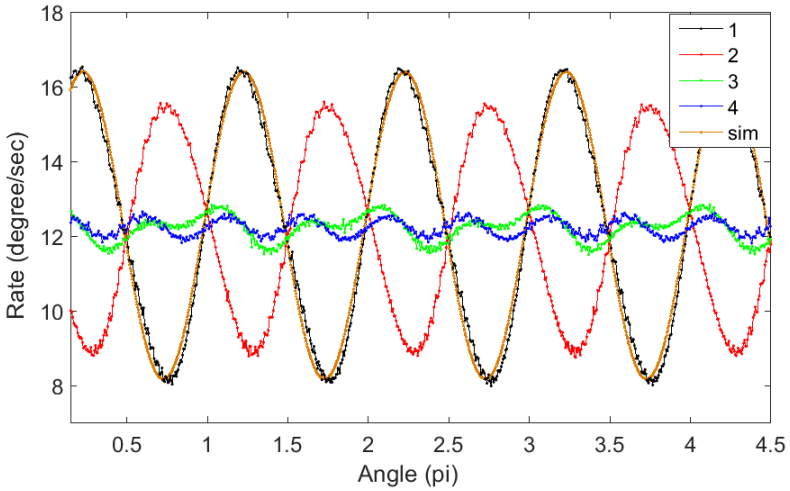

Figure 8, At constant input rate, precession rate fluctuates periodically along precession angle due to gyroscope imperfections. A simulation plot is also included.

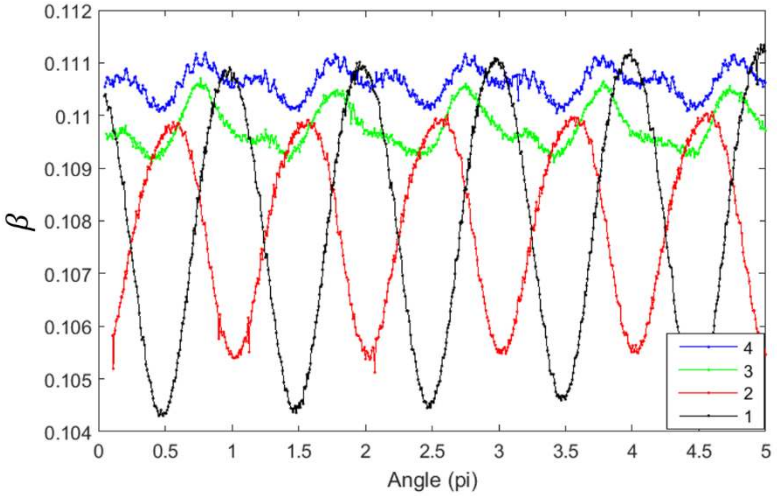

Figure 9, Control gain for energy sustain fluctuates because damping varies along the precession angle.

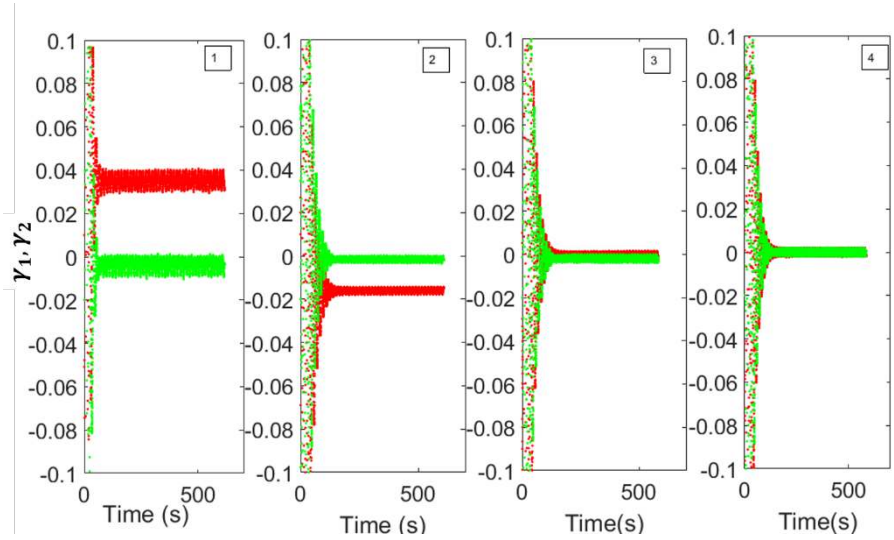

Figure 10, Damping imperfections are correctly estimated by the EKF for each scenario.

FFT of measured angular rate is shown in figure 11, which displays the second and fourth harmonics at the angle output. As shown in the approximate time averaged model (16)-(19), damping imperfections only result in second harmonics. This is confirmed in the figure that the fourth harmonic remains constant for all the 4 cases. The second harmonics dominates angle drift before damping compensation. However, it can be reduced by feedback control to a negligible level thereafter the fourth harmonic dominates. This shows the effectiveness of EKF based parameter estimation and feedback compensation of anisodamping using estimation results of the offline EKF. Rate threshold introduced using stiffness and damping imperfections [17][22] don't apply anymore when angle drift is dominated by 4^{th} harmonics caused by unmodelled dynamics.

Unlimited bandwidth, stable scale factor of RIGs are the fundamental advantages over rate gyroscopes. The EKF based anisodamping compensation is able to reduce the peak-to-peak angle drift to less than 1 degree per second. The upper cut-off rate for the RIG is determined by the DSP based electronic control loops, such as PID gains and sampling rate. As update rate for all the control loops is set at 1ms, it is reasonably expected the bandwidth of this RIG to be between 1/360 Hz to 100 Hz.

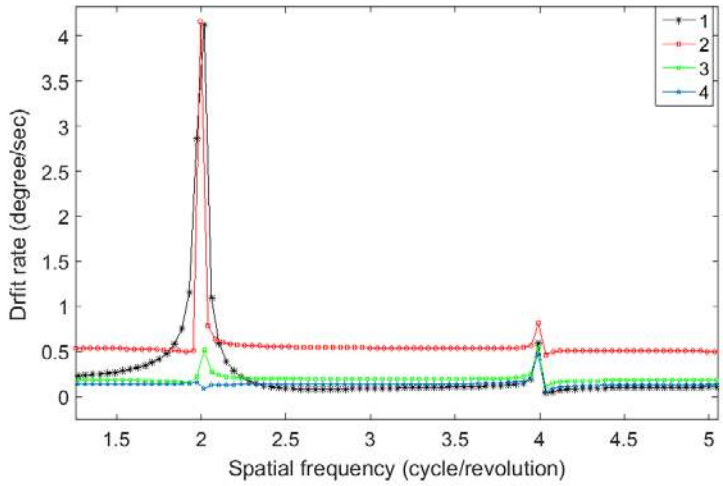

Figure 11, Harmonic analysis of angle output showing 2^{th} and 4^{th} harmonics.

8. Conclusions

Parameter identification of a MEMS vibratory gyroscope is an essential prerequisite for any adaptive control and state feedback compensation to minimize output errors. This paper described an offline EKF approach to this problem based on the slow varying averaged dynamic model. Because the system states and measurements are slow time varying, it is possible for the EKF to use a low update rate without causing excessive error in the linearization approximation of the system dynamics and affecting the instability of the EKF. Moreover, the observed measurements used in the estimation have significantly less noise thanks to the narrowband demodulation process. These advantages lead to an EKF for MEMS gyroscope with improved accuracy, stability and suitable for real time implementation. Numeric simulation validates the proposed algorithms with fast convergence and great accuracy. Offline application of the EKF with experimental gyroscope operation data also shows consistent results. Estimated damping parameters from the EKF are effectively used for a DSP based real time RIG control system to set the correct amount of feedback to compensate the non-proportional damping presents in the gyroscope. The angular drift has been reduced from 10 ^{o}/s to 1 degree per second, where the non-proportional damping caused 2^{th} harmonic error has been reduced to a negligible level, and the 4^{th} harmonics dominates.

Acknowledgment

The authors wish to acknowledge the support from K Townsend, C Gregory and A Kazer of UTAS (Plymouth,UK) to this research project in terms of the provision of hardware, and insightful discussions.

Reference

[1]. S. Park, R. Horowitz, and C. W. Tan. Dynamics and control of a MEMS angle measuring gyroscope. *Sensors and Actuator*, Vol. 144, Issue 1 (2008) 56-63.
[2]. Sungsu Park. Adaptive control of a vibratory angle measuring gyroscope. *Sensors*, Vol. 10, No. 9 (2010) 8478-8490.
[3]. J. A. Gregory, J. Cho, and K. Najafi. Novel mismatch compensation methods for rate-integrating gyroscopes. Position Location and Navigation Symposium (PLANS), 2012 IEEE/ION.
[4]. Z X Hu, B J Gallacher. Control and Damping Imperfection Compensation for a Rate Integrating MEMS Gyroscope. *DGON* Inertial *Sensors and Systems, September, 2015.*
[5]. Parsa Taheri-Tehrani; A. Dorian Challoner; Oleg Izyumin; Bernhard Boser; David Horsely. A new electronic feedback compensation method for rate integrating gyroscopes. IEEE International Symposium on Inertial Sensors and Systems. Laguna Beach, CA. 22-25 Feb. 2016.
[6]. R. M. C. Mestrom, R. H. B. Fey, J. T. M. van Beek, K. L. Phan, and H. Nijmeijer. Modelling the dynamics of a MEMS resonator: Simulations and experiments. *Sensors and Actuators A*: Physical, vol. 142, pp. 306–315, 2007.
[7]. Robert T. M'Closkey, Steve Gibson, Jason Hui. System Identification of a MEMS Gyroscope. *Journal of Dynamic system, measurement, and Control,* 123(2), 201-210, 1999.
[8]. Painter, C. C. and Shkel, A. M. Identification of anisoelasticity for electrostatic "trimming" of rate integrating gyroscope, SPIE Annual InternationalSymposium on Smart Structures and Materials, New Port Beach, CA., Vol. March, 2001.
[9]. A. Srikantha Phani, and Ashwin A Seshia. Identification of aniso-elasticity, non-proportional damping in MEMS gyroscopes. NSTI-Nanotech 2004.
[10]. Claus-Peter Fritzen. Identification of Mass, Damping and Stiffness Matrices of Mechanical Systems. Journal of Vibration, Acoustics, Stress, and Reliability in Design. 108(1):9, 1986.
[11]. Bernard Friedland. A Nonlinear Observer for Estimating Parameters in Dynamic Systems. Automatica, Vol. 33, Issue 8, (1997), 1525–1530.
[12]. Jaehwan Pi and Hyochoong Bang. Imperfection Parameter Observer and Drift Compensation Controller Design of Hemispherical Resonator Gyros. International Journal of Aeronautical and space science, Vol. 14, No.4 (2013) 379-386.
[13]. Ladislav Král, Miroslav šimandl. Parameter Estimation of MEMS Gyroscope Using Local State Estimation Methods. 17th IFAC Symposium on System Identification SYSID, Beijing, China, 19–21 October 2015.
[14]. Chien-Yu Chi, Yen-Pin Peng, and Tsung-Lin Chen. Compensation of Interface Circuit Errors for MEMS Gyroscopes Using State Observers. 3rd International Conference on Sensing Technology, Nov. 30 – Dec. 3, 2008, Taiwan.
[15]. Amir Ostadi, Moosa Ayati. Application of extended kalman filter to parameter identification of micro gyroscope. The 4th International conference on acoustic and vibration, Dec. 10-11, 2014.
[16]. Simon J. Julier, Jeffrey K. Uhlmann. A New Extension of the Kalman Filter to Nonlinear systems. Proceedings of SPIE, Signal Processing, Sensor Fusion, and Target Recognition VI, 28 July 1997.
[17]. B J Gallacher. Principles of a rate integrating gyroscope. IEEE Transactions on Aerospace and Electronic Systems. Vol.48, No. 1, 2012.
[18]. B. Friedland and M.F. Hutton. Theory and error analysis of vibrating-member gyroscope. *IEEE Transactions on Automatic Control,* Vol. 23, No. 4, 1978.
[19]. D.D. Lynch. Vibratory Gyro Analysis by the Method of Averaging. International conference on Gyroscopic Technology and Navigation, 1995, St. Petersburgh.
[20]. Andrei M. Shkel, Roberto Horowitzn. Dynamics and Control of Micromachined Gyroscopes. Proceedings of the American Control Conference. San Diego, California June 1999.
[21]. Z X Hu, B J Gallacher, Burdess J, Bowles SR. A systematic approach for precision electrostatic mode tuning of a MEMS gyroscope. Journal of Micromechanics and Microengineering. Vol14, Issue 12(2014), 125003.
[22]. Igor P. Prikhodko, Jeffrey A. Gregory, Dmitry I. Bugrov, Michael W. Judy. Overcoming Limitations of Rate Integrating Gyroscopes by Virtual Rotation. 2016 IEEE International Symposium on Inertial Sensors and Systems, Laguna Beach, CA. 22-25 Feb. 2016.